



Nocturnal cooling in Local Climate Zone: Statistical approach using mobile measurements

François Leconte, Julien Bouyer, Rémy Claverie

► To cite this version:

François Leconte, Julien Bouyer, Rémy Claverie. Nocturnal cooling in Local Climate Zone: Statistical approach using mobile measurements. Urban Climate, 2020, 33, pp.100629. 10.1016/j.uclim.2020.100629 . hal-02572122v1

HAL Id: hal-02572122

<https://hal.univ-lorraine.fr/hal-02572122v1>

Submitted on 22 Aug 2022 (v1), last revised 16 Jan 2023 (v2)

HAL is a multi-disciplinary open access archive for the deposit and dissemination of scientific research documents, whether they are published or not. The documents may come from teaching and research institutions in France or abroad, or from public or private research centers.

L'archive ouverte pluridisciplinaire **HAL**, est destinée au dépôt et à la diffusion de documents scientifiques de niveau recherche, publiés ou non, émanant des établissements d'enseignement et de recherche français ou étrangers, des laboratoires publics ou privés.



Distributed under a Creative Commons Attribution - NonCommercial 4.0 International License

Nocturnal cooling in Local Climate Zone: statistical approach using mobile measurements

Francois Leconte^{a,b,*}, Julien Bouyer^{b,*}, Rémy Claverie^b

^a *Université de Lorraine, Inra, LERMaB, F-88000, Épinal, France*

^b *Cerema Est, Team research group, F-54510, Tomblaine, France*

Abstract

Up-to-date climate scenarios warn that the frequency and intensity of heat waves are likely to increase in Europe during the twenty first century. In these circumstances, urban climate is progressively taken into account in urban planning processes, for instance using terrain classifications. The developed methodology involves the Local Climate Zone scheme (LCZ), which has been applied to Nancy, France. Mobile measurements campaigns have been performed using an instrumented vehicle in order to record daily air temperature dynamics, with a focus on the daily cooling period. So as to quantify LCZ cooling before and after sunset over several days, a climatic indicator called Normalized Cooling Rate (NCR) has been used. This study presents statistical regressions that have been performed between normalized cooling rate values calculated from field measurements and urban indicators. Results indicate that normalized cooling rates and most of the studied urban features are correlated. Regression model using sky view factor and distance

*Corresponding authors

Email addresses: francois.leconte@univ-lorraine.fr (Francois Leconte), julien.bouyer@cerema.fr (Julien Bouyer), remy.claverie@cerema.fr (Rémy Claverie)

to the city center seems enough accurate to estimate nocturnal cooling at the district scale.

Key words: Urban Heat Island, Air temperature, Mobile measurements, Nocturnal cooling, Local Climate Zone, Urban indicators, Regression analysis

1. Introduction

Urban Heat Island, that could be described as the increased air temperature in the city centers canopies compared to their surrounding rural spaces, has been recognized since the 1970s (Oke, 1973) and is now a well studied anthropic climatic phenomenon (Arnfield, 2003) (Gartland, 2008). Indeed, it has been identified as a major concern for public policies to mitigate it or to build up adaptation strategies facing it (Rizwan et al., 2008), for now and for the next decades when heat waves would be more frequent. UHI need to be more documented and understood by stakeholders and planners to better integrate it in their projects and applications, especially at the district scale (Grimmond et al., 2010) (Baklanov et al., 2018).

The UHI magnitude is both influenced by regional climatic and geographical parameters and instant meteorological data - that can be qualified as uncontrollable variables - and by city morphology, materials, land use and anthropogenic sources - that can be qualified as controllable variables (Rizwan et al., 2008).

In order to perform accurate city climate diagnosis, modelling approaches are improving continuously (Mirzaei, 2015). Surface Energy Balance in meteorological meso-scale models is the more relevant technique to deal with

20 physical processes both from the district to the city scale (Grimmond et al.,
21 2010) (Grimmond et al., 2011). But, these kind of model require at least
22 a high level of expertise held by researchers or technical engineers with a
23 strong background in climatology, or even, depending on the accuracy of
24 model parametrisation, well-supplied urban databases.

25 To take into account climate processes in a first approach, many empiri-
26 cal and statistical modelling of UHI have been investigated. Firstly Oke
27 proposed a method to link UHI maximum intensity with population and
28 incident wind, and due to the impact of city morphology, improve it by a
29 function of aspect ratio parameter (Oke, 1987). This approach has been
30 pursued by several studies involving sky view factor (Unger, 2004) (Svens-
31 son, 2004), a combination of urban indicators (Balázs et al., 2009) or hybrid
32 method between meteorological data and urban indicators (Bernard et al.,
33 2017).

34 Other researches tend to discriminate urban features using terrain clas-
35 sification such as the Urban Climate Zone (Oke, 2006) and more recently
36 the Local Climate Zone (LCZ) scheme (Stewart and Oke, 2012) to describe
37 inner urban climate. Measurements campaigns have highlighted that LCZ
38 demonstrate a homogeneous thermal behavior (Leconte et al., 2015) (Stewart
39 et al., 2013).

40 Decision makers are looking for models involving urban indicators that
41 provide quantitative information about thermal behavior of districts. This
42 work aims to develop correlations between LCZ indicators and UHI climatic
43 descriptors. This paper addresses specifically the methodology of statistical
44 analysis and the limits associated to the consistency of LCZ indicators.

45 2. Materials and methods

46 2.1. Mobile measurements within Local Climate Zone

47 2.1.1. Climate classification in Nancy

48 The conurbation of Nancy is located North East of France and numbers
49 286,000 inhabitants. It has an area of approximately 270 km² and its ele-
50 vation ranges between 190 meters and 420 meters. Regarding its geographic
51 features, Nancy is surrounded by two plateaus located West and North East
52 of the conurbation, and crossed by two water bodies from South East to
53 North. The Great Nancy Area is located in the center of the Lorraine re-
54 gion, which exhibits an temperate climate without dry season (Class Cfb
55 according to the Köppen-Geiger classification (Peel et al., 2007)).

56 The Local Climate Zones (LCZ) classification has been applied for the
57 area of interest. The determination of LCZ is organized following a three-
58 steps method. The contours of the LCZ have been determined based on
59 land use and building height information as well as global knowledge of the
60 experimental field. Over the conurbation of Nancy, 82 urbanized LCZ have
61 been identified.

62 2.1.2. LCZ selection for the field experiment

63 Thirteen LCZ of similar elevation have been selected, representing five
64 different LCZ types. Within these areas, seven urban indicators have been
65 calculated, namely sky view factor, aspect ratio, mean building height, ter-
66 rain roughness class, building surface fraction, impervious surface fraction
67 and pervious surface fraction. Contours have been corrected and a LCZ type
68 has been assigned to each of these thirteen LCZ regarding urban indicators

69 values (Table 1). Residential areas of Nancy presents urban features at the
70 edge between two LCZ types, namely "Open Lowrise" and "Sparsely Built".
71 It appears that urban indicators calculations did not allow to choose between
72 these two LCZ types, therefore three residential areas have been classified as
73 dual type "Open Lowrise / Sparsely Built".

74 *2.1.3. Field survey with instrumented vehicle*

75 On the basis of this LCZ map, screen-height air temperature has been
76 recorded within these thirteen LCZ during summer 2013 and 2015 (Figure
77 1). Mobile measurements have been performed using an instrumented vehicle
78 that records air temperature every three meters. A PT100 probe has been
79 placed within a ventilated cylinder, which has been mounted on the roof of
80 the car. This probe has an elevation of two meters above the ground, and
81 an accuracy of 0.2 °C. Data corresponding to very low speed measurements
82 may be influenced by heat release from other vehicles, therefore measures
83 carrier out below 15 km.h⁻¹ are dismissed. Since the itinerary is mostly
84 urban, the maximum vehicle speed is around 60 km.h⁻¹. A sensitivity test
85 has been performed in order to study the impact of vehicle speed on air
86 temperature. Results demonstrate that mean air temperature values are
87 marginally impacted by vehicle speed.

88 The chosen meteorological conditions are low wind speed (below 9 m.s⁻¹,
89 wind speed at 10 m high), clear sky (from 0 to 2 octas), anticyclonic condi-
90 tions, dry road and absence of precipitation during the previous twenty-four
91 hours. Regarding these requirements, seven measurements days have been
92 selected. Two measurements hours have been set, which correspond approx-
93 imately to the beginning of the cooling phase (5 PM local time) and to the

94 expected urban heat island amplitude maximum (three to five hours after
95 sunset, 0 PM local time) (Oke, 1987). A measurement takes approximately
96 two hours and thirty minutes, and during this time the regional temperature
97 can decrease up to 2 °C at night. A linear time-correction scheme has been
98 applied in order to balance the temperature evolution between the beginning
99 and the end of the measure session. The scheme consists in correcting the
100 measured air temperature proportionally to the elapsed time between the
101 beginning of the session and the measurement.

102 *2.2. Nocturnal cooling indicator at district scale*

103 This study focuses on the air temperature behavior at the individual Local
104 Climate Zones unit, which means that spatially averaged air temperature
105 is considered. The spatial homogeneity inside LCZ has been analyzed in
106 previous study (Leconte et al., 2015). The daily air temperature cycle is
107 specially investigated. The air temperature difference between two Local
108 Climate Zones is often used to characterize their thermal pattern. However,
109 temperature difference only provides information at a given time of the day.
110 In order to analyse the evolution throughout the time, heating rates or cooling
111 rates can be implemented. These rates are calculated as the derivative of air
112 temperature by the time.

113 Heating and cooling rates can be considered as urban climatic indica-
114 tors to examine the urban heat island phenomenon. For city located in the
115 same climate than Nancy, the urban heat island amplitude is generally weak
116 during daytime and strong during nighttime. This phenomenon starts to
117 develop before sunset and reach a maximum at night. Therefore, the cooling
118 period is the relevant period to study the urban heat island. For low cloud

cover and low wind speed, Holmer has observed that the cooling of neighborhoods is divided into two different phases (Holmer et al., 2007). During a first phase, urban areas show different cooling dynamics while during the second phase, the air temperature dynamics tend to be uniform between urban zones. The first phase coincides with a time period between one to two hours before sunset and three to five hours after sunset (P1 on Figure 2), while the second phase covers a period between three to five hours after sunset to sunrise (P2 on Figure 2). This two-phases cooling has been observed for several locations, namely in Singapore (Chow and Roth, 2006), Adelaide, Australia (Erell and Williamson, 2007), Athens, Greece (Giannopoulou et al., 2010), Ouagadougou, Burkina Faso (Holmer et al., 2013), Novi Sad, Serbia (Milosevic et al., 2019), and Nancy, France (Leconte et al., 2017). These previous results highlight that the amplitude of the urban heat island rises during phase 1 and remains stable during phase 2. Neighborhoods demonstrate different cooling rates during phase 1 and similar cooling rates during phase 2. In order to explicit the thermal behavior of Local Climate Zones during the development of the urban heat island, cooling rates during phase 1 are examined. The cooling rate are calculated between the daytime measure (character D on Figure 2) and the nighttime measures (character N on Figure 2). They are defined as :

$$\chi_{DN} = \frac{\Delta T_{air,DN}}{\Delta t_{DN}} \quad (1)$$

With Δt_{DN} the elapsed time between the two measures and $\Delta T_{air,DN}$ the air temperature decrease between the two measures for a given LCZ.

The diurnal temperature range (DTR) is expressed as the temperature difference between daily maximum and daily minimum temperature. It ap-

143 pears that cooling rates are not identical from one day to another due to
 144 diurnal temperature range variation. Thus, cooling rates during phase 1
 145 have been normalized in order to be able to compare them when several days
 146 show dissimilar DTR values. When several Local Climate Zones are studied,
 147 the cooling rates are divided by the temperature drop observed in the coolest
 148 Local Climate Zone during phase 1 ($\Delta T_{air,DN,max}$). In this way, all cooling
 149 rates – named normalized cooling rates (NCR) – are expressed relatively to
 150 an identified reference, namely the coolest studied area :

$$NCR = \frac{\chi_{DN}}{\Delta T_{air,DN,max}} \quad (2)$$

151 2.3. Statistical approach

152 In order to question the existence of a linear relationship between normal-
 153 ized cooling rate and urban indicators (UI), a regression analysis (ordinary
 154 least squares method) has been carried out. The regression model is evalu-
 155 ated by using both the regression coefficient to estimate the linearity and the
 156 Breusch-Pagan test to check if the variance around the regression line is the
 157 same for all values of the predictor (homoscedasticity) (Breusch and Pagan,
 158 1979).

159 Nine urban indicators have been selected. Seven of them belong to the
 160 LCZ scheme, namely sky view factor (SVF), aspect ratio (AR), mean build-
 161 ing height (H), terrain roughness class (R), building surface fraction (Built),
 162 impervious surface fraction (Imper), pervious surface fraction (Per). In ad-
 163 dition, the distance to the center of the conurbation (Pos) and the elevation
 164 (Elev) have also been examined, as they may impact the thermal behavior
 165 of the districts. The statistical results have been evaluated according three
 166 criteria:

- The regression coefficient of the linear regression between NCR and one (or more) urban indicator is used to evaluate the regression quality. A correlation coefficient close to one corresponds to an accurate regression model.
- Akaike Information Criteria (AIC) is applied on regression equations in order to compare them. This criterion is defined as equation (3). (Akaike, 1981) (Akaike, 1998)

$$\text{AIC} = 2K - 2\log(\ell(\hat{\theta}|y)) \quad (3)$$

Where K is the number of parameters to be estimated and $\log(\ell(\hat{\theta}|y))$ is the log likelihood at its maximum likelihood estimator $\hat{\theta}$ based on y observations. The most effective model is the model with the lowest AIC score. This approach has been used in previous studies for statistical model selection, including in the geosciences field (Gopalan et al., 2018) (Bernard et al., 2017).

- Student's t-test has been performed for each UI's coefficient of the linear regression in order to evaluate their contribution. The significance threshold chosen for the P-value is 0.05.

Regression calculations have been completed over a sample representing 75% of the normalized cooling rate values which has been chosen randomly. The remaining values (25% of the experimental data set) have been used to examine the quality of the regression equation. Thus, NCR estimations from empirical models are compared with independent NCR observations. The goodness of fit is estimated with the Chi-Square statistic (eq 4). As depicted

189 in this equation, the Chi-Square statistic (χ^2) is based on the difference be-
 190 tween the NCR observed during field measurements and the NCR estimated
 191 using the statistical models.

$$\chi^2 = \sum \frac{(NCR_{Obs.} - NCR_{Est.})^2}{NCR_{Est.}} \quad (4)$$

192 The lower the Chi-Square value, the better the NCR estimated value.

193 **3. Results and discussion**

194 *3.1. Single urban indicator approach*

195 Regressions have been performed between NCR and each of the nine
 196 studied urban indicator UI_i ($i \in \llbracket 1, 9 \rrbracket$), according to equation (5).

$$NCR = \beta_0 + UI_i \cdot \beta_1 \quad (5)$$

197 The constants β_0 and β_1 are the intercept and the slope of the linear regression
 198 respectively.

199 The relationship between NCR and urban indicators have been investi-
 200 gated based on 75% of the 90 experimental data set which has been chosen
 201 randomly. Initial dataset included measurements performed during seven
 202 days within thirteen LCZ (91 NCR values). One NCR value has been re-
 203 moved from the dataset due to experimental dysfunction. In order to as-
 204 sess the accuracy of this approach, the impact of the sample selection on
 205 regression results have been analysed. Multiple samples have been chosen
 206 randomly and then used to perform regression between NCR and urban in-
 207 dicators. The number of random samples is twice larger than the amount of
 208 field observations.

Figure 3 highlights that terrain roughness class, sky view factor, mean building height and the distance to the center of the conurbation achieve the lowest AIC values. The box plots for each urban indicator tend to be similar in terms of interquartile range and distance between extremum values.

Overall, it seems that indicators related to the urban morphology perform better than land use indicators. Indeed, urban morphology indicators are ranked in 1st, 2nd, 4th and 7th positions in terms of AIC values, while land use indicators are ranked in 5th, 6th and 8th positions.

After this step, one of the 180 random samples is selected, a regression is performed and it confirms the results of Figure 3 in terms of ranking. Table 2 summarizes the values of β_0 and β_1 coefficients as well as P-values, AIC and R^2 for one random sample. Thus, this sample will be used for following analysis. Results show that all Breusch-Pagan values are positives, which demonstrate the homoscedasticity of the data. All coefficients pass the Student's t-test, except in the case of the elevation. Based on AIC and R^2 values, the terrain roughness class is the indicator that leads to the best correlation with normalized cooling rate values ($AIC = -362.4$, $R^2 = 0.48$), followed by the sky view factor ($AIC = -359.2$, $R^2 = 0.45$) and the distance to the center of the conurbation ($AIC = -358.1$, $R^2 = 0.45$). The model that achieves the best results is presented in equation (6).

$$NCR = 0.17 \cdot R - 0.001 \quad (6)$$

Scatter plots of experimental data including regression lines are presented (Figure 4). Each graph presents NCR values, in relation to urban indicators calculated within the each of the thirteen identified LCZ, for seven days of measurements. First, a significant dispersion of NCR values can be noticed

233 for each of the urban indicators, between 0.04 and 0.06 h⁻¹. Nonetheless, all
 234 the scattered charts show trends of monotonic increase or decrease, except
 235 for the elevation indicator ($R^2 = 0.09$) mostly because the measurement
 236 surveys have been carried out at almost constant elevation. This allows us to
 237 elaborate basic conclusions confirming previous studies which express local
 238 intensity of heat island as a linear function of the SVF (Svensson, 2004). The
 239 graphs show patterns of vertical alignments of dots corresponding to the seven
 240 days of measurements in each of thirteen LCZ. For several indicators such as
 241 AR, SVF or Imper, clusters can be perceived because same LCZ typologies
 242 lead to very close indicator values (cf. Table 1). This is even more obvious
 243 for R that shows only four distinct values of terrain roughness class. Indeed,
 244 R is calculated using the Davenport classification (Davenport et al., 2000),
 245 which implies that R values are integers (cf. Table 1). The thirteen studied
 246 LCZ in Nancy belong to only four roughness class. On the other hand, for the
 247 position indicator, a slightly more homogeneous horizontal distribution can
 248 be observed, except for the two LCZ D (Low plants) located at the outskirts
 249 of the city.

250 In order to evaluate the regression equation related to the urban indica-
 251 tors, NCR computed from statistical regressions has been confronted with
 252 NCR obtained from the measurement validation data set (Figure 5). χ^2 val-
 253 ues are also calculated. The lower the χ^2 value, the closer the points from
 254 the first bisector. For the nine models, χ^2 values range from 0.02 to 0.065.
 255 The best results are obtained for the Sky View Factor (0.02), the distance to
 256 the center (0.02), the mean building height (0.022) and the terrain roughness
 257 class (0.022). Results presented in Figure 5 are consistent with AIC and R^2

values. Indeed, urban indicators with the lowest AIC values and the highest R^2 show the lowest χ^2 values. The elevation of all the studied LCZ is quite similar. Since the NCR varies depending on the LCZ, the regression between NCR and Elev leads to poor results. Thus, the parameter Elev will not be taken into account for the following section.

Finally, the single urban indicator approach allows to identify urban indicators that explain best the NCR variations. However, nocturnal cooling of LCZ is led by multiple factors. Therefore, a multiple urban indicators approach have to be investigated in order to propose a more comprehensive model.

3.2. Multiple urban indicators approach

Multiple linear regression are investigated between NCR and several urban indicators (Eq. (7)).

$$\text{NCR} = \beta_0 + \sum_{p=1}^{p=n} UI_p \cdot \beta_p \quad (7)$$

A collinearity analysis of the urban indicators is carried out. A strong level of collinearity between independent variables can lower the performance of the statistical model. Correlation matrix between the eight urban indicators has been calculated (Figure 6). 82% of the correlation coefficients are above 0.7, which highlights that many indicators are strongly correlated.

The high level of correlation observed in Figure 6 is explained by the morphological and layout patterns of the neighborhoods. Indeed, an increase of sky view factor value may be linked to a decrease of built surface fraction and mean building height. The LCZ position in the conurbation (Pos) is also

280 correlated with morphological and land use indicators. This result may be
281 due to the specific spatial distribution of the LCZ types for the studied area.
282 Within the Nancy conurbation, the most dense areas with highest building
283 height and built surface fraction are located in the center, while the less
284 dense areas with moderate building height and low built surface fraction can
285 be found close to the conurbation's boundaries. Therefore, an increase of
286 the radial distance from the center of the conurbation can correspond to an
287 urbanisation gradient.

288 Explanatory variables can be considered as weakly correlated if the cor-
289 relation coefficient ranges between -0.5 and $+0.5$. It appears that only one
290 pair of urban indicators reaches this criteria, namely the impervious surface
291 fraction with the aspect ratio. However, regarding the single indicator ap-
292 proach (cf. Section 3.1 and Table 2), these two indicators demonstrate poorer
293 correlation with NCR (higher AIC and lower R^2) than other indicators. As
294 a result, this pair (i.e. impervious surface fraction and aspect ratio) seems
295 to be not relevant for a regression involving two indicators.

296 This analysis suggests that in the case of multi indicator regression, only
297 a small number of urban indicators can be selected in order to lower the
298 negative effects of the collinearity. The choice of these urban indicators is
299 based on urban and statistical criteria.

300 First, it appears that urban indicators can be sorted depending on their
301 nature. Sky view factor, aspect ratio, mean building height and terrain
302 roughness class are related to the urban morphology, while the built, imper-
303 vious and pervious surface fraction refer to the urban land use. The distance
304 to the center of the conurbation can be considered as independent geograph-

ical indicator. If the two urban indicators selected for the regression belong to the same group, the model may be redundant and the other group will not be represented. Therefore, the two selected indicator should be chosen in different groups.

Second, indicators that demonstrate low AIC values for single indicator regression can be selected for multiple variables regression. For the land use group, the pervious surface fraction has been selected. Unlike the built and impervious surface fraction, this indicator provides an indirect information regarding the vegetation. Regarding the urban morphology group, R and SVF show the best AIC values. The later is selected for the multiple indicator regressions because it describes the urban geometry in a more detailed way than the terrain roughness class, which is based on the Davenport classification. The distance to the center has been selected due to its low AIC value.

Three urban indicators – namely SVF, Per and Pos – are then selected to carry out regressions. Four regressions are presented, namely:

- Three regressions between NCR and two explanatory variables (combinations of SVF, Per and Pos)
- One regression between NCR and three explanatory variables

Models are discussed regarding their χ^2 value (cf. section 2.3). Figure 7 presents NCR calculated from the observations in function of NCR estimated by regressions in the multiple variables regression case. χ^2 ranges from 0.016 to 0.02. Among the two indicators model, the pair SVF and Pos obtains the lowest χ^2 value (0.016). This can be considered as an improvement regarding

the single variable regression approach, which only reach a χ^2 value of 0.02. Finally, the two indicators model which leads to the better estimation of the normalized cooling rate is expressed in equation (8).

$$NCR = 4.7 \times 10^{-3} \cdot Pos + 4.4 \times 10^{-5} \cdot Per + 8.8 \times 10^{-2} \quad (8)$$

In addition, a model involving these three indicators is proposed. Regression model involving three urban indicators – namely SVF, Per and Pos – do not achieve better performance ($\chi^2 = 0.016$).

4. Conclusion

This paper questions the relationship between the cooling pattern of districts and several urban indicators. This study has required the application of the Local Climate Zone scheme in Nancy. During this stage, nine urban indicators have been determined within a selection of thirteen LCZ. Nocturnal cooling information has been gathered throughout measurement campaigns, and normalized cooling rate have been calculated based on these field data.

The statistical connection between NCR and the chosen urban indicators have been investigated using regression analysis. The statistical models are built using 75% of the total experiments. The overall performance of the urban indicators (i.e. AIC values) is independent from the sample. Nine single variable regressions are presented. Terrain roughness class, the sky view factor, the mean building height and the distance to the center of the conurbation achieve best results in terms of AIC, R^2 and χ^2 .

Multi indicator regressions have been investigated in order to take into account multiple drivers of the LCZ nocturnal cooling. Correlations appear

351 to be generally strong between urban indicators, which limits the number of
352 explanatory variables for the regression. Three urban indicators are selected
353 for the multiple indicator regression. The best results are obtained with
354 the pair SVF and Pos. The addition of a third explanatory variable do not
355 improve the performance of the model.

356 Regression analysis underlines the general trends regarding the relation-
357 ship between normalized cooling rate and the nine selected urban indicators.
358 Overall, it looks like NCR and most of the studied urban features are corre-
359 lated. However, morphological indicators seems to perform better than land
360 use indicators.

361 **Acknowledgments**

362 This work has been supported by the French Environment and Energy
363 Management Agency (ADEME).

364 **References**

- 365 Akaike, H., 1981. Likelihood of a model and information criteria. *Journal of*
366 *Econometrics* 16 (1), 3 – 14.
- 367 Akaike, H., 1998. *Information Theory and an Extension of the Maximum*
368 *Likelihood Principle*. Springer New York, New York, NY, pp. 199–213.
- 369 Arnfield, A., 2003. Two decades of urban climate research: a review of tur-
370 bulence, exchanges of energy and water, and the urban heat island. *Inter-*
371 *national Journal of Climatology* 23, 1–26.

372 Baklanov, A., Grimmond, C., Carlson, D., Terblanche, D., Tang, X.,
373 Bouchet, V., Lee, B., Langendijk, G., Kolli, R., Hovsepyan, A., 2018.
374 From urban meteorology, climate and environment research to integrated
375 city services. *Urban Climate* 23, 330 – 341, iCUC9: The 9th International
376 Conference on Urban Climate.

377 Balázs, B., Unger, J., Gál, T., Sümeghy, Z., Geiger, J., Szegedi, S., 2009.
378 Simulation of the mean urban heat island using 2D surface parameters:
379 empirical modelling, verification and extension. *Meteorological Applica-*
380 *tions* 16, 275–287.

381 Bernard, J., Musy, M., Calmet, I., Bocher, E., Keravec, P., 2017. Urban
382 heat island temporal and spatial variations: Empirical modeling from ge-
383 ographical and meteorological data. *Building and Environment* 125, 423 –
384 438.

385 Breusch, T. S., Pagan, A. R., 1979. A simple test for heteroscedasticity and
386 random coefficient variation. *Econometrica* 47 (5), 1287–1294.

387 Chow, W., Roth, M., 2006. Temporal dynamics of the urban heat island of
388 Singapore. *International Journal of Climatology* 26, 2243–2260.

389 Davenport, A., Grimmond, C., Oke, T., Wieringa, J., 2000. Estimating the
390 roughness of cities and sheltered country. In: *Proceedings of the 12th Con-*
391 *ference of Applied Climatology*.

392 Erell, E., Williamson, T., 2007. Intra-urban differences in canopy layer air
393 temperature at a mid-latitude city. *International Journal of Climatology*
394 27, 1243–1255.

395 Gartland, L., 2008. Heat Island : Understanding and Mitigating Heat in
396 Urban Areas. Earthscan.

397 Giannopoulou, K., Santamouris, M., Livada, I., Georgakis, C., Caouris, Y.,
398 2010. The impact of canyon geometry on intra urban and urban suburban
399 night temperature differences under warm weather conditions. Pure and
400 Applied Geophysics 167, 1433–1449.

401 Gopalan, S., Kawamura, A., Takasaki, T., Amaguchi, H., Azhikodan, G.,
402 2018. An effective storage function model for an urban watershed in terms
403 of hydrograph reproducibility and akaike information criterion. Journal of
404 Hydrology 563, 657–668.

405 Grimmond, C., Blackett, M., Best, M., Baik, J.-J., Belcher, S., Beringer,
406 J., Bohnenstengel, S., Calmet, I., Chen, F., Coutts, A., Dandou, A., For-
407 tuniak, K., Gouvea, M., Hamdi, R., Hendry, M., Kanda, M., Kawai, T.,
408 Kawamoto, Y., Kondo, H., Krayenhoff, E., Lee, S.-H., Loridan, T., Mar-
409 tilli, A., Masson, V., Miao, S., Oleson, K., Ooka, R., Pigeon, G., Porson,
410 A., Ryu, Y.-H., Salamanca, F., Steeneveld, G.-J., Tombrou, M., Voogt, J.,
411 Young, D., Zhang, N., 2011. Initial results from phase 2 of the international
412 energy balance model comparison. International Journal of Climatology 31,
413 244–272.

414 Grimmond, C., Roth, M., Oke, T., Au, Y., Best, M., Betts, R., Carmichael,
415 G., Cleugh, H., Dabberdt, W., Emmanuel, R., Freitas, E., Fortuniak, K.,
416 Hanna, S., Klein, P., Kalkstein, L., Liu, C., Nickson, A., Pearlmutter,
417 D., Sailor, D., Voogt, J., 2010. Climate and more sustainable cities: cli-

418 mate information for improved planning and management of cities (produc-
419 ers/capabilities perspective). *Procedia Environmental Sciences* 1, 247–274.

420 Holmer, B., Thorsson, S., Eliasson, I., 2007. Colling rates, sky view fac-
421 tors and the development of intra-urban air temperature differences. *Ge-*
422 *ografiska Annaler Series A - Physical Geography* 89, 237–248.

423 Holmer, B., Thorsson, S., Lindén, J., 2013. Evening evapotranspirative cool-
424 ing in relation to vegetation and urban geometry in the city of Oua-
425 gadougou, Burkina Faso. *International Journal of Climatology* 33, 3089–
426 3105.

427 Leconte, F., Bouyer, J., Claverie, R., Pétrissans, M., 2015. Using Local Cli-
428 mate Zone scheme for UHI assessment: evaluation of the method using
429 mobile measurements. *Building and Environment* 83, 39–49.

430 Leconte, F., Bouyer, J., Claverie, R., Pétrissans, M., Oct 2017. Analysis of
431 nocturnal air temperature in districts using mobile measurements and a
432 cooling indicator. *Theoretical and Applied Climatology* 130 (1), 365–376.

433 Milosevic, D., Savic, S., Arsenovic, D., Secerov, I., Matzarakis, A., 2019.
434 Quantication of temporal changes of urban heat island intensity and cool-
435 ing and heating rates in dierent local climate zones of mid-sized central
436 european city (tromp foundation travel award). In: *Proceedings of the*
437 *EMS Annual Meeting* 2019.

438 Mirzaei, P. A., 2015. Recent challenges in modeling of urban heat island.
439 *Sustainable Cities and Society* 19, 200 – 206.

- 440 Oke, T., 1973. City size and the urban heat island. *Atmospheric Environment*
441 (1967) 7 (8), 769 – 779.
- 442 Oke, T., 1987. *Boundary Layer Climate*, 2nd Edition. Routledge.
- 443 Oke, T., 2006. Toward better scientific communication in urban climate.
444 *Theoretical and Applied Climatology* 84, 179–190.
- 445 Peel, M., Finlayson, B., McMahon, T., 2007. Updated world map of the
446 Köppen-Geiger climate classification. *Hydrology and Earth System Sci-*
447 *ences* 11, 1633–1644.
- 448 Rizwan, A., Dennis, Y., Liu, C., 2008. A review on the generation, deter-
449 mination and mitigation of urban heat island. *Journal of Environmental*
450 *Sciences* 20, 120–128.
- 451 Stewart, I., Oke, T., 2012. Local Climate Zones for urban temperature stud-
452 ies. *Bulletin of American Meteorology Society* 93, 1879–1900.
- 453 Stewart, I., Oke, T., Krayenhoff, E., 2013. Evaluation of the 'Local Climate
454 Zone' scheme using temperature observations and model simulations. *In-*
455 *ternational Journal of Climatology* (DOI: 10.1002/joc.3746).
- 456 Svensson, M., 2004. Sky view factor analysis - implications for urban air
457 temperature differences. *Meteorological Applications* 11, 201–211.
- 458 Unger, J., 2004. Intra-urban relationship between surface geometry and ur-
459 ban heat island: review and new approach. *Climate Research* 27, 253–264.

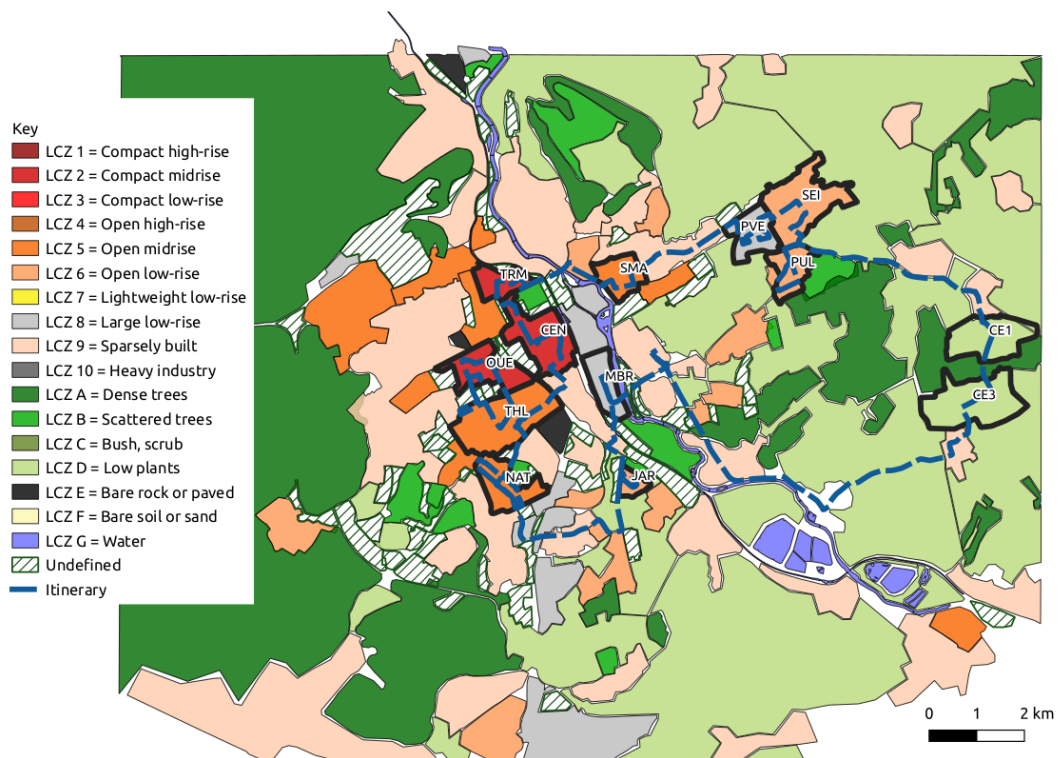


Figure 1: LCZ map of the Great Nancy Area. The itinerary is displayed in blue. The thirteen selected LCZ for the field experiment are circled in black.

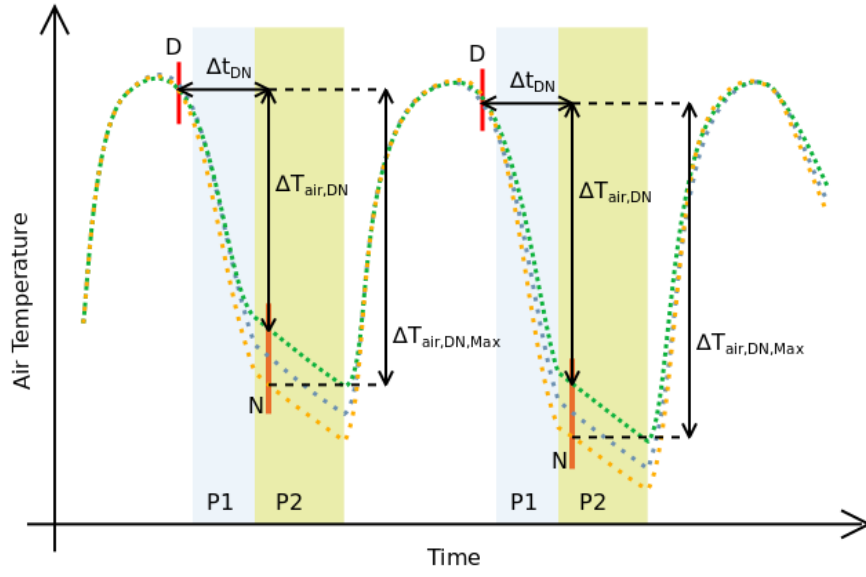


Figure 2: Theoretical nocturnal cooling phases for three LCZ of different types. Phase 1 (P1, blue area) is between 1 to 3 h before sunset and 3 to 5 h after sunset. Phase 2 (P2, green area) is between 3 and 5 h after sunset and sunrise. The letter D refers to the sessions performed in the middle of the afternoon, letter N refers to the sessions carried out around 3 h after sunset.

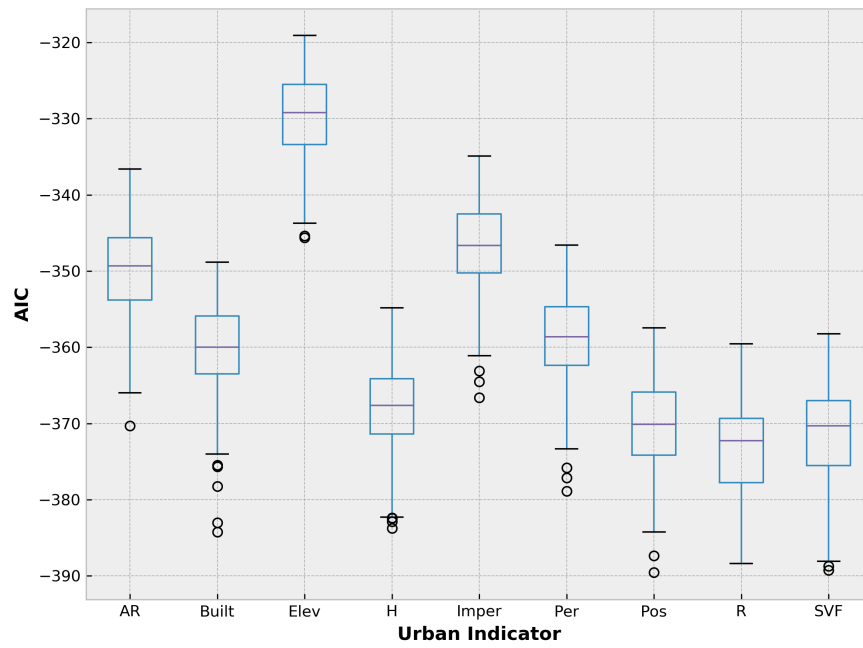


Figure 3: AIC values calculated from 180 different models for each urban indicator. Each model is based on 75% of the experimental data set which has been chosen randomly.

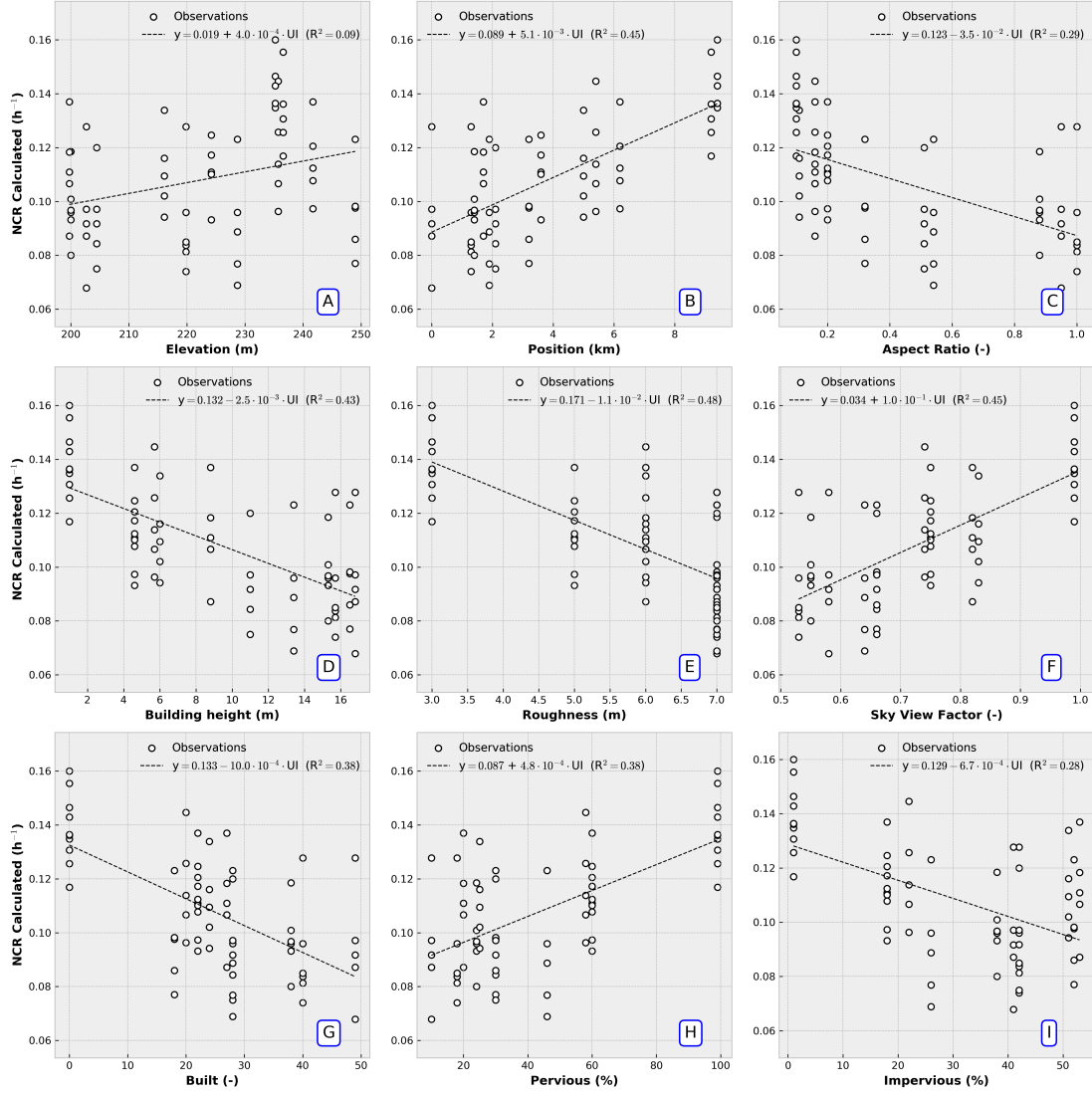


Figure 4: Scatter plots of experimental data including regression lines. Each observation correspond to a particular day for a given LCZ. Values with identical abscissa refer to a specific LCZ.

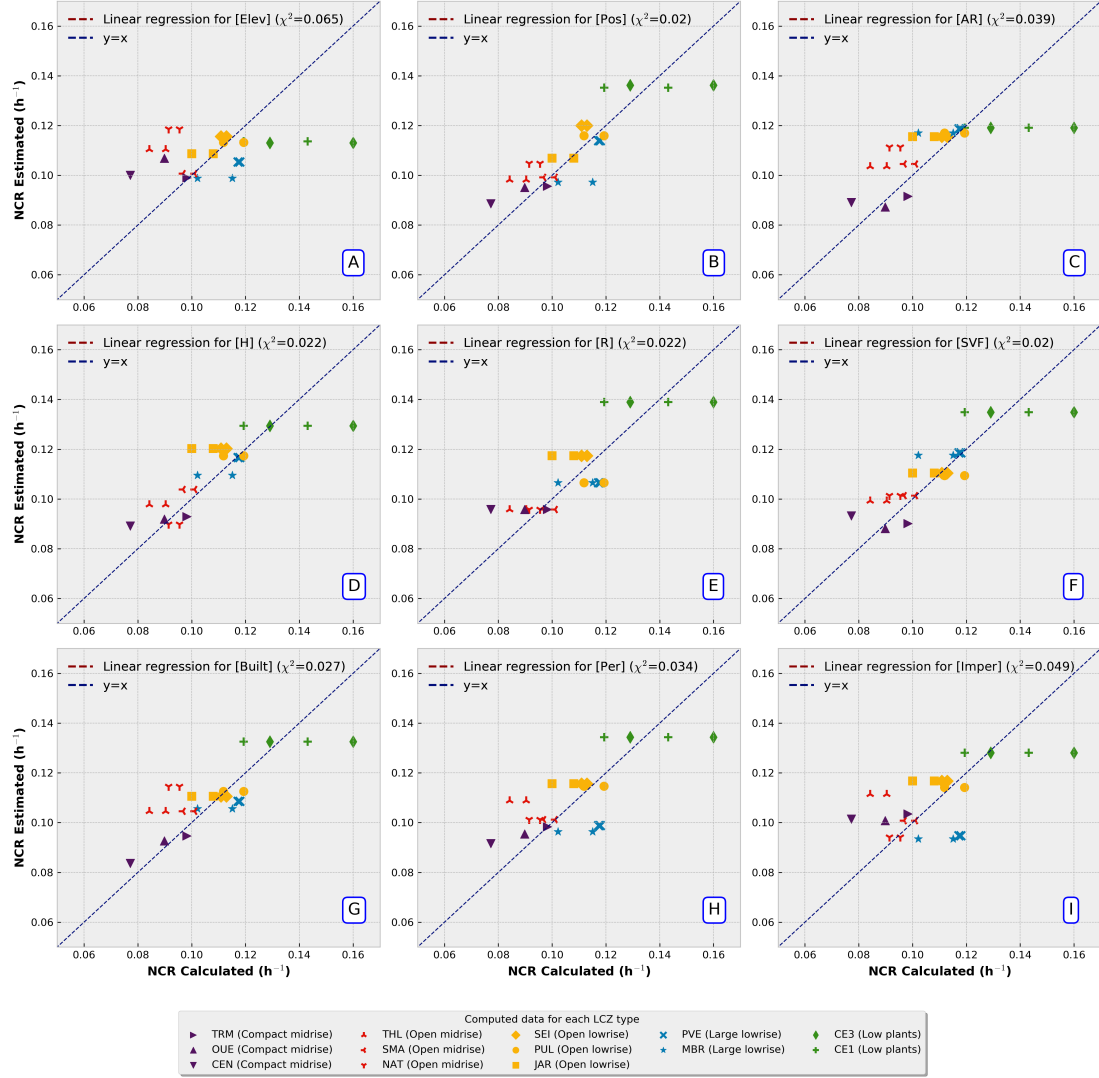


Figure 5: NCR from statistical regressions compared with NCR from the validation data set for single indicator regression. If the models would estimate perfectly the NCR from the validation data set, all the points would be on the first bisector (blue dashed line).

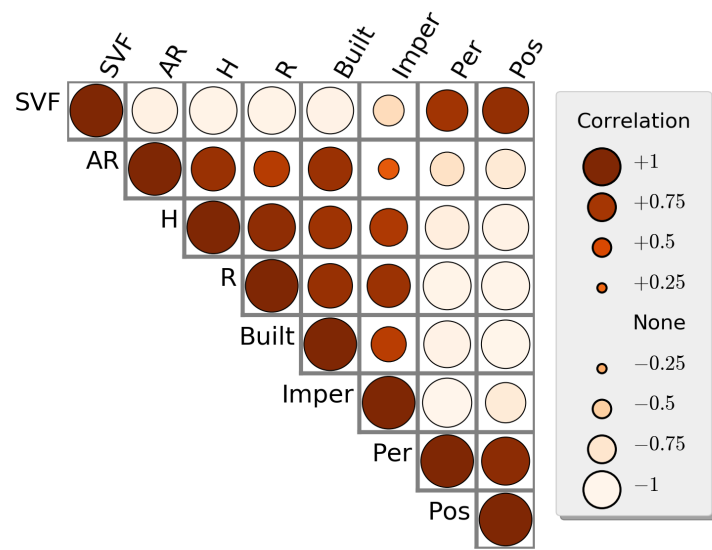


Figure 6: Correlation matrix of the explanatory variables, namely the urban indicators. The bigger the dot, the larger the correlation coefficient. The color indicates the sign of the correlation (positive/negative).

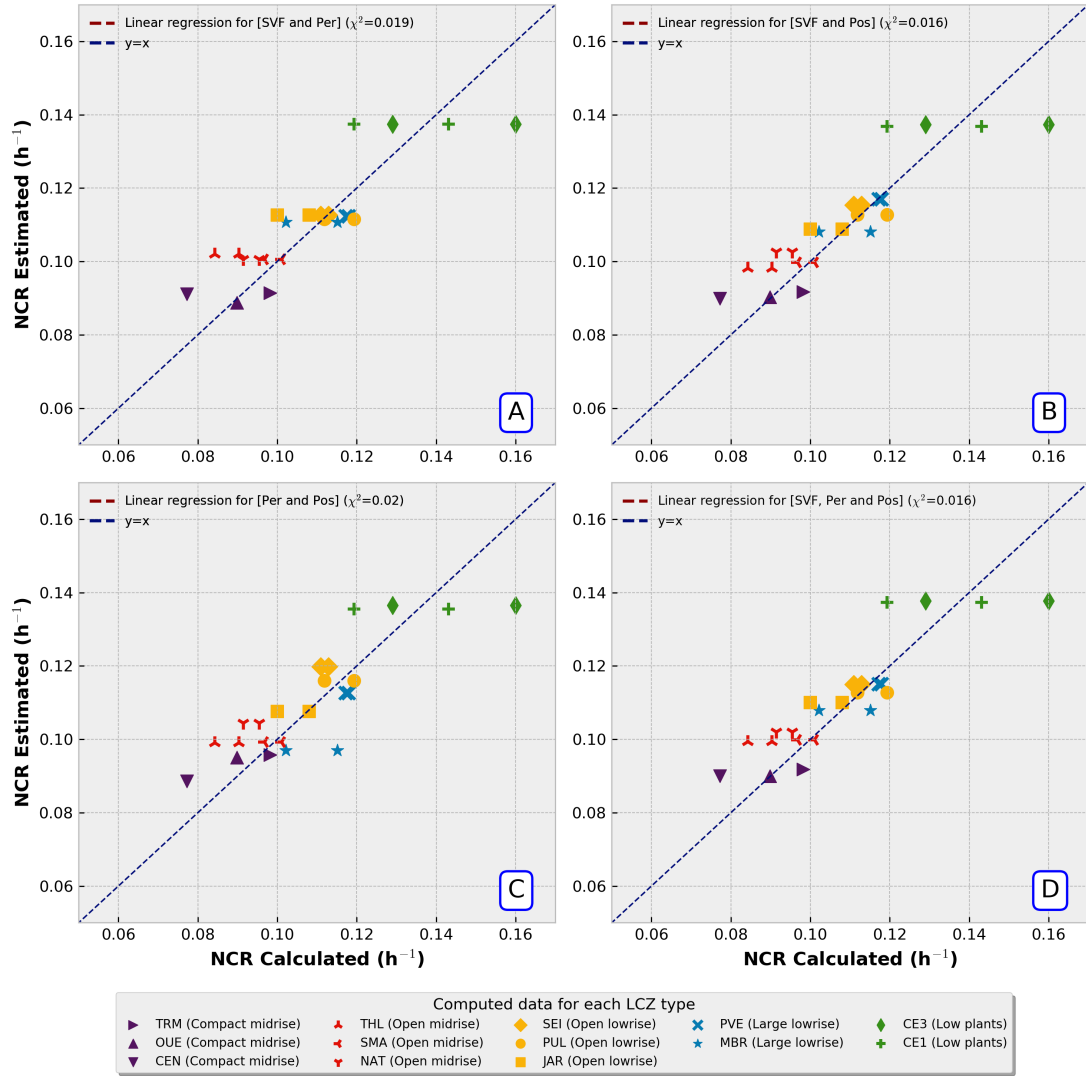


Figure 7: NCR from statistical regressions compared with NCR from the validation data set for multiple indicator regression. If the models would estimate perfectly the NCR from the validation data set, all the points would be on the first bisector (blue dashed line).

LCZ code	SVF (-)	AR (-)	H (m)	R (-)	Built (%)	Imper (%)	Per (%)	LCZ type (-)
OUE	0.53	1.00	15.7	7	40	42	18	2 (Compact Midrise)
CEN	0.58	0.95	16.8	7	49	41	10	2 (Compact Midrise)
TRM	0.55	0.88	15.3	7	38	38	24	2 (Compact Midrise)
NAT	0.66	0.32	16.5	7	18	52	30	5 (Open Midrise)
THL	0.64	0.54	13.4	7	28	26	46	5 (Open Midrise)
SMA	0.66	0.51	11.0	7	28	42	30	5 (Open Midrise)
MBR	0.82	0.16	8.8	6	27	53	20	8 (Large Lowrise)
PVE	0.83	0.11	6.0	6	24	51	25	8 (Large Lowrise)
JAR	0.75	0.20	4.8	5	22	18	60	6 / 9 (Open Lowrise / Sparsely Built)
SEI	0.75	0.16	5.0	6	19	22	59	6 / 9 (Open Lowrise / Sparsely Built)
PUL	0.74	0.16	5.7	6	20	22	58	6 / 9 (Open Lowrise / Sparsely Built)
CE1	> 0.9	< 0.1	< 1	3	0	1	99	D (Low Plants)
CE3	> 0.9	< 0.1	< 1	3	0	1	99	D (Low Plants)

Table 1: Urban indicators values for the thirteen selected LCZ. SVF: Sky view factor, AR: Aspect ratio, H: Mean building height, R: Terrain roughness class, Built: Built surface fraction, Imper: Impervious surface fraction, Per: Pervious surface fraction.

Urban Indicator	β_0	$P > t $	β_1	$P > t $	AIC	R^2	P_{BP}
R	0.17	$< 10^{-3}$	-0.01	$< 10^{-3}$	-362.43	0.48	0.21
SVF	0.03	$< 10^{-3}$	0.10	$< 10^{-3}$	-359.22	0.45	0.31
Pos	0.09	$< 10^{-3}$	0.01	$< 10^{-3}$	-358.13	0.45	0.12
H	0.13	$< 10^{-3}$	-0.00	$< 10^{-3}$	-356.79	0.43	0.42
Per	0.09	$< 10^{-3}$	0.00	$< 10^{-3}$	-350.83	0.38	0.20
Built	0.13	$< 10^{-3}$	-0.00	$< 10^{-3}$	-350.24	0.38	0.38
AR	0.12	$< 10^{-3}$	-0.04	$< 10^{-3}$	-341.93	0.29	0.85
Imper	0.13	$< 10^{-3}$	-0.00	$< 10^{-3}$	-340.39	0.28	0.28
Elev	0.02	0.59	0.00	0.01	-324.80	0.09	0.07

Table 2: Coefficients (β_0 and β_1), Student's t-test ($P > |t|$), Akaike Information Criteria and R^2 regarding regressions between normalized cooling rate and nine explanatory variables. Student's t-test results need to be under the chosen threshold of 0.05, whereas Breusch-Pagan values must be different from zero.